Controlled Correlation and Squeezing in $Pr^{3+}:Y_2SiO_5$ to Yield Correlated Light Beams

Changbiao Li,[1] Zihai Jiang,[1] Yiqi Zhang,[1] Zhaoyang Zhang,[1] Feng Wen,[1] Haixia Chen,[1] Yanpeng Zhang,[1,*] and Min Xiao[2,3,†]

[1]*Key Laboratory for Physical Electronics and Devices of the Ministry of Education and Shaanxi Key Lab of Information Photonic Technique, Xi'an Jiaotong University, Xi'an 710049, China*

[2]*Department of Physics, University of Arkansas, Fayetteville, Arkansas 72701, USA*

[3]*National Laboratory of Solid State Microstructures and School of Physics, Nanjing University, Nanjing 210093, China*

(Received 26 March 2016; revised manuscript received 23 November 2016; published 30 January 2017)

We report the generation of twin beams by the parametric amplification four-wave mixing process and triplet beams by the parametric amplification six-wave mixing (PA SWM) process associated with the multiorder fluorescence signals in a $Pr^{3+}:Y_2SiO_5$ crystal. The intensity noise correlation and intensity-difference squeezing result from the nonlinear gain, which can be well controlled by the polarized dressing effect. The correlation value at the resonant position increases due to the double dressing effect; however, such correlation decreases if the triple dressing effect works. Specifically, correlation and squeezing between Stokes and anti-Stokes signals can be also switched by the relative nonlinear phase shift. The generated triplet beams from the PA SWM process have potential applications in three-mode all-optical information processing that can be used in on-chip photonic devices.

DOI: 10.1103/PhysRevApplied.7.014023

I. INTRODUCTION

As a further step towards integrated quantum photonic devices, it is necessary to miniaturize external light sources to improve their performance, such as their portability, stability, and multifunctionality. To achieve such light sources, methods that are based on traditional nonlinear optical crystals, especially domain-engineered quadratic nonlinear photonic crystals [1,2], were developed. Recently, a certain valuable extension of the path-entangled states to high-dimensional entanglement from a domain-cascaded lithium niobate crystal was reported [3]. On the other hand, rare-earth-doped crystals such as $Pr^{3+}:Y_2SiO_5$ exhibit unique features in comparison to nonlinear crystals. In these kinds of doped crystals, the "atomlike" properties of the dopant can be kept, in which the atomic coherence can be induced easily when interacting with multiple laser beams. As for the atomic coherence effects in solid-state materials, recent research includes electromagnetically induced transparency [4,5], light velocity reduction and coherent storage [6–8], optical quantum computing [9,10], all-optical routing based on optical storage [11], and enhanced four-wave mixing (FWM) based on atomic coherence [12], to name a few. It is worth mentioning that following the latest developments in intensity squeezed light with FWM in an atomic vapor, one can use the multiwave mixing processes in such rare-earth-doped crystals to generate entangled lights.

In this paper, we report the generation of correlated light beams from a parametric amplification four-wave-mixing (PA FWM) process and a PA six-wave-mixing (PA SWM) process in a $Pr^{3+}:Y_2SiO_5$ crystal. Two nonlinear cascade optical processes are controlled by adjustable dressing fields, and the results show that the degrees of the three-mode correlation and squeezing are induced by the dressed nonlinear gain. The correlation and squeezing can be controlled by the relative nonlinear phase shift caused by the dressing fields. On the other hand, the correlation and squeezing of PA FWM can be switched to anticorrelation and antisqueezing. Such controllable properties have potential applications in all-optical communication and optical information processing on photonic chips.

II. THEORETICAL MODEL

The sample is a 0.05% rare-earth Pr^{3+}-doped Y_2SiO_5 ($Pr^{3+}:Y_2SiO_5$) crystal, in which the triplet-energy-level $^3H_4$ and singlet-energy-level $^1D_2$ are selected to couple with each other. It is easy to identify the energy levels by investigating the optical spectrum of Pr^{3+}. The degeneracy of the Pr^{3+} energy levels is prohibited due to the crystal field of Y_2SiO_5; the $^3H_4$ and $^1D_2$ states are split into nine and five Stark components, respectively. The five relevant energy levels are δ_0 ($|0\rangle$ and $|1\rangle$), γ_0 ($|2\rangle$), δ_1 ($|3\rangle$), γ^*_0 ($|4\rangle$) in a five-level atomic system as shown in Fig. 1(a). The nature linewidths are about 2 kHz (site I) and 1 kHz (site II) [13]. The input laser beams are along the [010] axis of the

*Corresponding author.
ypzhang@mail.xjtu.edu.cn
†Corresponding author.
mxiao@uark.edu

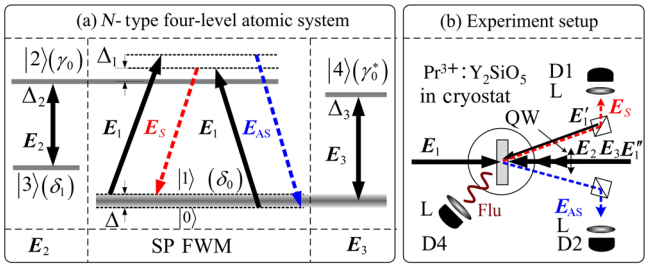

FIG. 1. Experimental setup. (a) N-type four-level atomlike system in $Pr^{3+}:Y_2SiO_5$. The width of ground state $|0\rangle$ represents the broadened degenerate states. (b) Experimental setup scheme. Flu, fluorescence; D, photomultiplier tube; L, lens. $\boldsymbol{E}_2$ and $\boldsymbol{E}_3$ counterpropagate with $\boldsymbol{E}_1$.

Y_2SiO_5 crystal, where the [010] axis is perpendicular to the optical axis. A strong pump beam $\boldsymbol{E}_1$ (frequency ω_1, wave vector $\mathbf{k}_1$, Rabi frequency G_1, wavelength 605.97 nm, coupling transition $|0\rangle \leftrightarrow |2\rangle$ with detuning $\Delta_i = \omega_{mn} - \omega_i$, $|1\rangle \leftrightarrow |2\rangle$ $\Delta_1' = \omega_{21} - \omega_1$, where ω_{mn} denotes the corresponding atomic transition frequency, and ω_i is the laser frequency), $\boldsymbol{E}_2$ (ω_2, $\mathbf{k}_2$,G_2, 609.27 nm, $|3\rangle \leftrightarrow |2\rangle$, Δ_2), and $\boldsymbol{E}_3$ (ω_3, $\mathbf{k}_3$, G_3, 607.96 nm, $|0\rangle \leftrightarrow |4\rangle$, Δ_3, $|1\rangle \leftrightarrow |4\rangle$, Δ_3'). The Pr^{3+} impurity ions occupy two nonequivalent cation sites (i.e., sites I and II) in the Y_2SiO_5 crystal. The energy levels for site I are labeled by a greek letter without an asterisk, while for site II by an asterisk, as shown in Fig. 1(a). Actually, with the induced dipole-dipole interaction considered, the coupling between the Pr^{3+} ions localized at different cation vacancies in the Y_2SiO_5 crystal can occur [14], so one can treat the two ions (at different sites) as a hetero-nuclear-like molecule. Therefore, one can establish an N-type four-level diagram ($|3\rangle \leftrightarrow |2\rangle \leftrightarrow |1\rangle \leftrightarrow |4\rangle$ or $|3\rangle \leftrightarrow |2\rangle \leftrightarrow |0\rangle \leftrightarrow |4\rangle$), which is composed of one Λ-type ($|3\rangle \leftrightarrow |2\rangle \leftrightarrow |0\rangle$ or $|3\rangle \leftrightarrow |2\rangle \leftrightarrow |1\rangle$) subsystem and one V-type ($|2\rangle \leftrightarrow |0\rangle \leftrightarrow |4\rangle$ or $|2\rangle \leftrightarrow |1\rangle \leftrightarrow |4\rangle$) subsystem. A two-photon coupling process can be implemented by the transition $|2\rangle \leftrightarrow |1\rangle \leftrightarrow |4\rangle$.

In the following theoretical section, we first introduce the nonlinear gain and then interpret that the intensity of such nonlinear gain can be controlled by the dressing effect. Based on the above, we investigate the intensity noise correlation and intensity-difference squeezing in the dressing PA FWM.

A. Spontaneously parametric FWM

The SP FWM process involves a coupled Stokes channel and an anti-Stokes channel and produces twin photons. One can express such SP FWM process with the Hamiltonian [15]

$$H = \frac{\kappa}{v}(\hat{a}^+\hat{b}^+ + \hat{a}\,\hat{b}), \tag{1}$$

where $\hat{a}^+(\hat{a})$ is the creation (-annihilation) operator that acts on the electromagnetic excitation of the $\boldsymbol{E}_S$ channel, whereas $\hat{b}^+(\hat{b})$ acts on the $\boldsymbol{E}_{\rm AS}$ channel. v is the group velocity of light in the nonlinear medium, and $\kappa_{S,\rm AS} = |-i\varpi_{S,\rm AS}\chi^{(3)}E_1^2/2|$ is the pumping parameter of the SP FWM, which depends on the nonlinearity $\chi^{(3)}$ and the pump-field amplitude. $\rho_{11}^{(0)}\overset{\omega_1}{\to}\rho_{21}^{(1)}\overset{\omega_{\rm AS}}{\to}\rho_{01}^{(2)}\overset{\omega_1}{\to}\rho_{21(S)}^{(3)}$ and $\rho_{00}^{(0)}\overset{\omega_1}{\to}\rho_{20}^{(1)}\overset{\omega_S}{\to}\rho_{10}^{(2)}\overset{\omega_1}{\to}\rho_{20(\rm AS)}^{(3)}$ are the central frequencies of the generated Stokes and anti-Stokes signals. Different from the case occurring in nonlinear crystals, $\chi^{(3)}$ is a function of the density-matrix elements. A SP FWM process occurs in the paraxial direction due to the so-called self-diffraction phase-matching FWM process generated in a "double-Λ-type" subsystem [$|0\rangle \leftrightarrow |1\rangle \leftrightarrow |2\rangle$ between two vertical dashed lines in Fig. 1(a)]. The strong pumping field $\boldsymbol{E}_1$ together with the generated Stokes ($\boldsymbol{E}_s$) and anti-Stokes ($\boldsymbol{E}_{\rm AS}$) fields satisfy the phase-matching conditions $\mathbf{k}_S = 2\mathbf{k}_1 - \mathbf{k}_{\rm AS}$ and $\mathbf{k}_{\rm AS} = 2\mathbf{k}_1 - \mathbf{k}_S$. Laser beams $\boldsymbol{E}_2$ and $\boldsymbol{E}_3$ (counterpropagating with $\boldsymbol{E}_1$) can cause resonant absorption and are used only to dress such SP FWM. Thus, only dressed SP FWM can be detected, and the generated fields can be described by the perturbation chains [16,17] $\rho_{11}^{(0)}\overset{\omega_1}{\to}\rho_{21}^{(1)}\overset{\omega_{\rm AS}}{\to}\rho_{01}^{(2)}\overset{\omega_1}{\to}\rho_{21(S)}^{(3)}$ ($\boldsymbol{E}_S$) and $\rho_{00}^{(0)}\overset{\omega_1}{\to}\rho_{20}^{(1)}\overset{\omega_S}{\to}\rho_{10}^{(2)}\overset{\omega_1}{\to}\rho_{20(\rm AS)}^{(3)}$ ($\boldsymbol{E}_{\rm AS}$). Therefore, one gets [18]

$$\rho_{21(S)}^{(3)} = -iG_{\rm AS}{}^*G_1{}^2/(d_{21}d_{01}d_{21}'), \tag{2}$$

$$\rho_{20(\rm AS)}^{(3)} = -iG_S{}^*G_1{}^2/(d_{20}d_{10}d_{20}'), \tag{3}$$

where $G_i = \mu_{ij}E_i/\hbar$ is the Rabi frequency of field $\boldsymbol{E}_i$ with the electric dipole matrix elements μ_{ij}, $d_{20} = \Gamma_{20} + i\Delta_1$, $d_{10} = \Gamma_{10} + i\delta$, $d_{20}' = \Gamma_{20} + i(\Delta_1 + \Delta + \delta)$, $d_{21} = \Gamma_{21} + i\Delta_1'$, $d_{01} = \Gamma_{01} - i\delta$, $d'_{21} = \Gamma_{21} + i(\Delta_1 - \delta)$, and Γ_{ij} is the decay rate between energy levels $|i\rangle$ and $|j\rangle$. The real frequencies of the generated Stokes and anti-Stokes signals can be expressed as $\omega_S = \varpi_S + \delta$ and $\omega_{\rm AS} = \varpi_{\rm AS} - \delta$ respectively, where the introduced symbol θ can be viewed as the criterion for the linewidths of the generated signal.

The boson-creation (-annihilation) operator satisfies the Heisenberg operator equation of motion in the dipole approximation:

$$d\hat{a}/dz = [\hat{a}, \hat{H}]/i\hbar = \kappa\hat{b}^+, \tag{4}$$

$$d\hat{b}^+/dz = [\hat{b}^+, \hat{H}]/i\hbar = \kappa\hat{a}. \tag{5}$$

After some algebra, we get the photon numbers of the Stokes and anti-Stokes field at the output site of the medium [15,19]:

$$\langle \hat{a}_{\rm out}^{+}\hat{a}_{\rm out}\rangle = \frac{1}{2}\left[\cos\left(2L\sqrt{AB}\sin\frac{\varphi_1+\varphi_2}{2}\right) + \cosh\left(2L\sqrt{AB}\cos\frac{\varphi_1+\varphi_2}{2}\right)\right]\frac{A}{B}, \quad (6)$$

$$\langle \hat{b}_{\rm out}^{+}\hat{b}_{\rm out}\rangle = \frac{1}{2}\left[\cos\left(2L\sqrt{AB}\sin\frac{\varphi_1+\varphi_2}{2}\right) + \cosh\left(2L\sqrt{AB}\cos\frac{\varphi_1+\varphi_2}{2}\right)\right]\frac{B}{A}, \quad (7)$$

where L is the medium length, $\rho_{21(S)}^{(3)} = Ae^{i\varphi_1}$, $\rho_{20(\rm AS)}^{(3)} = Be^{i\varphi_2}$, and A (B) and φ_1 (φ_2) are the modulus and phase angles of $\rho_{21(S)}^{(3)}$ ($\rho_{20(\rm AS)}^{(3)}$), respectively.

When three beams $\boldsymbol{E}_1$, $\boldsymbol{E}_1'$, and $\boldsymbol{E}_1''$ (from the same laser) are turned on [see Fig. 1(b)], a coherent FWM signal ($\mathbf{k}_F = \mathbf{k}_1 + \mathbf{k}_1'' - \mathbf{k}_1'$) is produced. If we inject this FWM signal into the Stokes channel of the SP FWM [14], we obtain the PA FWM. Therefore, the gain of the Stokes channel is given by

$$g = \frac{1}{2}\left[\cos\left(2L\sqrt{AB}\sin\frac{\varphi_1+\varphi_2}{2}\right) + \cosh\left(2L\sqrt{AB}\cos\frac{\varphi_1+\varphi_2}{2}\right)\right]. \quad (8)$$

B. Dressed PA FWM

Taking into account the dressing effects of $\boldsymbol{E}_2$ and $\boldsymbol{E}_3$, Eqs. (2) and (3) can be rewritten as [16]

$$\rho_{21(S)}^{(3)} = -iG_{\rm AS}{}^{*}G_1{}^{2}/(d_{21D}d_{01}d'_{21D}), \quad (9)$$

$$\rho_{20(\rm AS)}^{(3)} = -iG_S{}^{*}G_1{}^{2}/(d_{20D}d_{10}d'_{20D}), \quad (10)$$

where $d_{21D} = \Gamma_{21} + i(\Delta_1+\Delta) + |G_2|^2/[\Gamma_{31} + i(\Delta_1+\Delta-\Delta_2) + |G_1|^2/\Gamma_{11}]$, $d_{20D} = \Gamma_{20} + i\Delta_1 + |G_2|^2/[\Gamma_{30} + i(\Delta_1-\Delta_2) + |G_1|^2/\Gamma_{00}]$, $d'_{21D} = \Gamma_{21} + i(\Delta_1-\delta) + |G_3|^2/(\Gamma_{41}+i\Delta_3)$, $d'_{20D} = \Gamma_{20} + i(\Delta_1+\Delta+\delta) + |G_3|^2/(\Gamma_{40}+i\Delta_3)$.

In addition, the polarization of the dressing field ($\boldsymbol{E}_2$ or $\boldsymbol{E}_3$) can be controlled by a quarter-wave plate (QWP) [see Fig. 1(b)]. We assume the P-polarization direction (along an optic axis of the crystal) to be the quantization axis, so the component perpendicular to it (S polarization) is decomposed into balanced left- and right-circularly-polarized parts, while the component parallel to it (P polarization) remains linearly polarized. So, the dressing terms in Eqs. (9) and (10) are replaced by $C_{g2,\rm lin}^2(\cos^4\theta + \sin^4\theta)|G_2|^2$ and $C_{g2,\rm cir}^2(2\cos^2\theta\sin^2\theta)|G_2|^2$, respectively. Here, $C_{g,\rm lin}$ and $C_{g,\rm cir}$ are Clebsch-Gordan (CG) coefficients for linear and circular polarization, respectively [20]. θ is the rotated angle between the QWP's axis and P-polarization direction. Because of the relationship $\kappa \propto \chi_i^{(3)} \propto \rho^{(3)}$, the output signals of this PA FWM process can be manipulated by the dressing fields ($\boldsymbol{E}_2$ or $\boldsymbol{E}_3$), e.g., the power, frequency detuning, and polarization.

C. Intensity noise correlation and intensity-difference squeezing

The output number of photons is given by $\langle \hat{a}_{\rm out}^{+}\hat{a}_{\rm out}\rangle$, which is proportional to the intensity since $I \propto \langle \hat{a}_{\rm out}^{+}\hat{a}_{\rm out}\rangle$. The intensity fluctuation is $\delta\hat{I}(t) = \hat{I}(t) - \langle\hat{I}(t)\rangle$. Therefore, the correlation between the intensity fluctuations of the output Stokes and anti-Stokes PA FWMs fields [19,21] can be obtained

$$G_{S,\rm AS}^{(2)}(\tau) = \frac{\langle[\delta\hat{I}_S(t_S)][\delta\hat{I}_{\rm AS}(t_{\rm AS})]\rangle}{\sqrt{\langle[\delta\hat{I}_S(t_S)]^2\rangle\langle[\delta\hat{I}_{\rm AS}(t_{\rm AS})]^2\rangle}} = \frac{|\Psi_{S,\rm AS}|^2}{\sqrt{|C_S|^2|C_{\rm AS}|^2}}, \quad (11)$$

where $\tau = \tau_{\rm AS} - \tau_s$, $\tau_j = t_j - r_j/c$, r_j is the optical path from the output surface of the crystal to the jth detector ($j = 1, 2$), t_j is the trigger time, $\langle[\delta\hat{I}_S(t_S)][\delta\hat{I}_{\rm AS}(t_{\rm AS})]\rangle$ is the cross-correlation function between the intensity fluctuations of $\boldsymbol{E}_{\rm AS}$ and $\boldsymbol{E}_S$,$C_S = \sqrt{R_s}\int d\omega_S \sinh^2(\kappa L)$, $C_{\rm AS} = \sqrt{R_{\rm AS}}\int d\omega_{\rm AS}\sinh^2(\kappa L)$, V_Q is the quantization volume, and $R_{S,\rm AS} = V_Q^{1/3}E_{S,\rm AS}^2/(2\pi\nu_{S,\rm AS})$ are self-correlation functions of $\boldsymbol{E}_S$ and $\boldsymbol{E}_{\rm AS}$, respectively, where $\Psi_{S,\rm AS}(\tau) = i\pi E_1^2 E_S E_{\rm AS}\omega_1\int e^{-i\delta\tau}\chi^{(3)}(\delta)d\delta$.

Considering the Boltzmann distribution with finite temperature, the two-photon envelope function can be obtained by performing a Fourier transform on the third-order nonlinear susceptibility, $\Psi_{s-as}(\tau) = i\pi E_1^2 E_S E_{\rm AS}\omega_1\int e^{-i\delta\tau}\chi^{(3)}(\delta)d\delta = i\pi E_1^2 E_S E_{\rm AS}\omega_1/[(\Gamma_{21}+i\Delta_1+i\Delta)(i\Delta_1+\Gamma_{21}-\Gamma_{01})][e^{-\Gamma_-\tau} - e^{-i\Delta_1\tau}e^{-\Gamma_+\tau}]$ [22]. In addition, taking into account the interaction between the sample and coupling fields, the broadened linewidth of the measured SP FWM signal is $\Gamma_\pm = \Gamma_{\rm pop} - \Gamma(\pm\delta) + \Gamma_{\text{ion-spin}} + \Gamma_{\text{ion-ion}} + \Gamma_{\rm phonon}$, where $\Gamma_{\rm pop} = (2\pi T_1)^{-1}$ depends on the location of the energy level in phase space, with T_1 describing the population decay time, and the term $\Gamma(\pm\delta)$ represents the location of the energy level, which can be dressed by the coupling field. The last three terms ($\Gamma_{\text{ion-spin}} + \Gamma_{\text{ion-ion}} + \Gamma_{\rm phonon}$) are components of $(2\pi T_2^*)^{-1}$ (the reversible transverse relaxation time T_2^*). $\Gamma_{\text{ion-spin}}$ is related to the ion-spin coupling effect of the individual ion. $\Gamma_{\text{ion-ion}}$ is determined by the interaction among the rare-earth ions and can be controlled by the power of the external field and impurity concentration. $\Gamma_{\rm phonon}$ is related to the sample temperature. To quantify $\Gamma_{\text{ion-ion}}$, $P(t)$ is introduced $P(t)_a = \exp[-c_H\sum_{n=6,8,10,12,13,14}(A_{nH}/R_H^n)]$ and $P(t)_b = \exp[-c_D\sum_{n=5,6,7}(A_{nD}/R_D^n)]$, where A_{nH}/A_{nD} is the van der Waals attractive force coefficient, R_H^n/R_D^n is the distance of the nucleus, c_H and c_D represent

the population densities at the triplet energy level $^3H_4$ and singlet energy level $^1D_2$, respectively, and can be controlled by the pump power. $\sum(A_{nH}/R_H^n)$ and $\sum(A_{nD}/R_D^n)$ represent the induced dipole-dipole interaction of states H-H and D-D, respectively.

The degree of two-mode intensity-difference squeezing is given by [19,23,24]

$$\begin{aligned} \mathrm{sq} &= \log_{10}\frac{\langle\delta^2(\hat{I}_S-\hat{I}_{\mathrm{AS}})\rangle}{\langle\delta^2(\hat{I}_S+\hat{I}_{\mathrm{AS}})\rangle} \approx \log_{10}\frac{\langle\delta^2(\hat{N}_S-\hat{N}_{\mathrm{AS}})\rangle}{\langle\delta^2(\hat{N}_S+\hat{N}_{\mathrm{AS}})\rangle} \\ &= -\log_{10}(2g-1), \end{aligned} \tag{12}$$

where $\langle\delta^2(\hat{N}_S-\hat{N}_{\mathrm{AS}})\rangle$ is the mean square deviation of the intensity difference, and $\langle\delta^2(\hat{N}_S+\hat{N}_{\mathrm{AS}})\rangle$ is the mean square deviation of the intensity sum of the coherent laser beams.

D. Multiorder fluorescence

We adopt the perturbation theory to investigate the multiorder-fluorescence (MFL) signal [25,26]. When $\boldsymbol{E}_1$ and $\boldsymbol{E}_2$ are open, the MFL signal is generated in the Λ-type-level system of $Pr^{3+}:Y_2SiO_5$. Taking into account the dressing effects of $\boldsymbol{E}_1$ and $\boldsymbol{E}_2$ and the perturbation chains $\rho_{00}^{(0)}\overset{\omega_1}{\rightarrow}\rho_{20}^{(1)}\overset{-\omega_1}{\rightarrow}\rho_{22}^{(2)}\overset{-\omega_2}{\rightarrow}\rho_{32}^{(3)}\overset{\omega_2}{\rightarrow}\rho_{22}^{(4)}$, the intensity of MFL signal can be described by the diagonal density matrix element $\rho_{22}^{(4)}$, which is given by [14]

$$\begin{aligned} \rho_{\mathrm{MFL}}^{(4)} = \rho_{22}^{(4)} &= |G_2|^2|G_1|^2/[d_{20D}\Gamma_{00}d_{32} \\ &\times(\Gamma_{22}+|G_2|^2/d_{32}+|G_1|^2/d_{20})], \end{aligned} \tag{13}$$

where $d_{32}=\Gamma_{32}+i\Delta_2$.

III. RESULTS AND DISCUSSION

A. System preparation

The sample (a 3-mm $Pr^{3+}:Y_2SiO_5$ crystal) is held at 77 K in a cryostat (CFM-102). Three transform-limited tunable dye lasers (narrow scan with a 0.004-cm^{-1} linewidth) pumped by an injection-locked single-mode Nd: YAG laser (Continuum Powerlite DLS 9010, 10-Hz repetition rate, 5-ns pulse width) are used to generate the pumping fields $\boldsymbol{E}_1$, $\boldsymbol{E}_1'$, $\boldsymbol{E}_1''(\omega_1,\Delta_1)$, $\boldsymbol{E}_2(\omega_2,\Delta_2)$, and $\boldsymbol{E}_3(\omega_3,\Delta_3)$. The diameter of all beams is 0.8 mm. The polarizations of the laser beams are controlled by inserting wave plates into the corresponding beam paths. In such multilevel atomlike system, one can obtain the PA FWM with an injecting coherent FWM signal ($\mathbf{k}_F=\mathbf{k}_1+\mathbf{k}_1''-\mathbf{k}_1'$). Note that the generated signals ($\boldsymbol{E}_S$, $\boldsymbol{E}_{\mathrm{AS}}$) are quantum correlated [27,28]. Figure 1(b) shows the experimental arrangement taking into account the above phase-matching condition. The generated signals ($\boldsymbol{E}_S$, $\boldsymbol{E}_{\mathrm{AS}}$) are associated with MFL signals and detected by photomultiplier tubes. Such PA FWM process can be doubly dressed by applying dressing fields $\boldsymbol{E}_1$ and $\boldsymbol{E}_2$ (or $\boldsymbol{E}_3$) or triply dressed by applying all three dressing fields $\boldsymbol{E}_1$, $\boldsymbol{E}_2$, and $\boldsymbol{E}_3$ simultaneously.

B. Two-mode experimental results

Nonlinear processes can occur easily in the paraxial direction of the incident laser beam. In the current experiment, the PA FWM process occurs, which is well interpreted by a self-diffraction-type FWM process in which a strong pumping field $\boldsymbol{E}_1$ is mixed with two weak fields $\boldsymbol{E}_S$ and $\boldsymbol{E}_{\mathrm{AS}}$ as shown in Fig. 1(a) (middle panel). The parameter space to be searched for in our investigation of the dressed PA FWM together with the MFL is large, with the frequency detuning Δ_1 of pumping field $\boldsymbol{E}_1$ and the powers and the polarization states of both dressing fields $\boldsymbol{E}_2$ and $\boldsymbol{E}_3$ as externally controlled variables. In addition, we compare the dressing effects of two structures in Fig. 1(a), i.e., $\boldsymbol{E}_2$ dressing in a Λ-type three-level subsystem of an individual Pr^{3+} ion and $\boldsymbol{E}_3$ dressing in a V-type three-level subsystem of a hetero-nuclear-like molecule.

Since the generated $\boldsymbol{E}_S$ and $\boldsymbol{E}_{\mathrm{AS}}$ are twin beams and have similar properties, we choose only $\boldsymbol{E}_S$ and its MFL to show the properties under various dressing conditions. First of all, we analyze the accompanied MFL spectra [see Fig. 2(a)] under various dressing conditions in the Λ-type subsystem. The typical linewidths of MFL signals are about 30 GHz. On the one hand, they are broadened by phonons (Γ_{phonon}) from the lattice heat vibration and the power ($\Gamma_{\mathrm{ion\text{-}ion}}$) of the pumping field. On the other hand, they are balanced by the dressing effect [$\Gamma(\pm\delta)$] [29]. At a relatively low power of $P_1=1$ mW [Fig. 2(a1)], the MFL has a Lorentzian line shape with a small Autler-Townes (AT) splitting [14], which is induced by setting $P_2=3$ mW. One way to explain these observed effects is by using the dressed-stated picture.

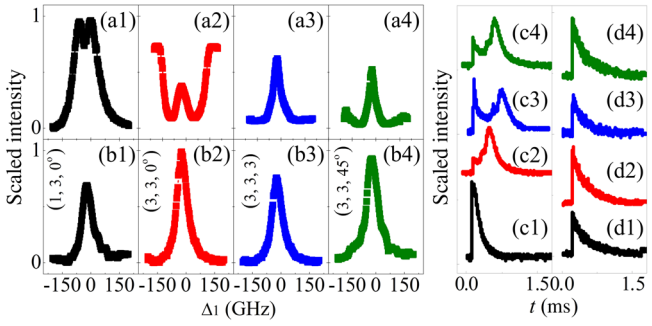

FIG. 2. Measurements of the PA FWM ($\boldsymbol{E}_S$) and MFL excitation spectra associated with their lifetimes under specified experimental parameters. (a)–(d) Dressed spectra and lifetimes. (a) The MFL spectra, (b) the PA FWM spectra $\boldsymbol{E}_S$, (c) temporal MFL, and (d) $\boldsymbol{E}_S$ intensity. The parameters inside the parentheses in (b1), (b2), and (b4) are $\boldsymbol{E}_1$ power, $\boldsymbol{E}_2$ power, and $\boldsymbol{E}_2$ polarization by QWP, where the linear and circular polarizations are denoted as $\theta=0°$ and $\theta=45°$ of the QWP, respectively. In (b3), the parameters are $\boldsymbol{E}_1$ power, $\boldsymbol{E}_2$ power, and $\boldsymbol{E}_3$ power. $G_1=25$ GHz at 3 mW.

The power of $\boldsymbol{E}_2$ splits the energy level $|2\rangle$ into $|G_{2\pm}\rangle$. From the Hamiltonian equation $H|G_{2\pm}\rangle = \lambda_{\pm}|G_{2\pm}\rangle$, we obtain $\lambda_{\pm} = [\Delta_2 \pm (\Delta_2{}^2 + 4|G_2|^2)^{1/2}]/2$. Therefore, the splitting distance between $|G_{2\pm}\rangle$ is $2\sqrt{\Delta_2^2 + 4|G_2|^2}$, as shown in Fig. 2(a1). Next, by increasing $P_1 = 3$ mW [Fig. 2(a2)], the MFL is suppressed by the double-dressing effect of $\boldsymbol{E}_1$ and $\boldsymbol{E}_2$ which appears as a suppression dip [see Eq. (13)]. Here, the baseline comes from another fluorescence process excited by $\boldsymbol{E}_2$. Physically, this phenomenon can be attributed to the nest-type dressing term d_{20} in Eq. (13) [14,20]. The suppressing ability of $\boldsymbol{E}_1$ increases as the detuning Δ_1 gets closer to resonance. However, this situation changes at the resonant region of $\Delta_1 = \Delta_2 = 0$, in which a peak of $\boldsymbol{E}_S$ due to the high power of $\boldsymbol{E}_1$ overlaps with the dip. Third, when $\boldsymbol{E}_2$ and $\boldsymbol{E}_3$ are both turned on simultaneously, the triple-dressing effect must be considered. As demonstrated in Fig. 2(a3), the MFL is suppressed completely. If the beam $\boldsymbol{E}_2$ is set to be circularly polarized [Fig. 2(a4)] while all other parameters remain the same as those in Fig. 2(a2), one can easily see that the dressing effect in such case is stronger than that in the linear case in Fig. 2(a2). Since the CG coefficients may be different for different transitions between Zeeman sublevels, the Rabi frequency can vary with polarization even if the frequency and power of the laser field remain unchanged. For example, the CG coefficients, $C_{g,\mathrm{cir}}$ (circular polarization) and $C_{g,\mathrm{lin}}$ (linear polarization) are $\sqrt{4/35}$ and $\sqrt{1/35}$, respectively with $M = 1/2$. So, the dressing terms in Eq. (13) are replaced by $C_{g2,\mathrm{lin}}^2(\cos^4\theta + \sin^4\theta)|G_2|^2$ and $C_{g2,\mathrm{cir}}^2(2\cos^2\theta\sin^2\theta)|G_2|^2$, respectively. Thus, the ratio between dressing term of the circular and linear case is expressed as $C_{g2,\mathrm{cir}}^2/C_{g2,\mathrm{lin}}^2 = 4$, with $\theta = 45°$ and $M = +1/2$, which indicates that the dressing effects in the circularly polarized subsystems are far greater than those in the linearly polarized subsystems.

In addition, one can find that the dressed state, one of the most important consequences of the dressing effect of beam $\boldsymbol{E}_2$, makes the intensity curves in the time domain with $\Delta_1 = \Delta_2 = 0$ show double peaks of the AT splitting configuration. There exist two peaks, which correspond to the locations of the zero delay time and a longer delay time [30], as displayed in Figs. 2(c2)–2(c4). The obvious delay of the right peak in Fig. 2(c1) is caused by the residual particles in $|G_{2+}\rangle$ transferring to $|G_{2-}\rangle$ through phonon-assisted nonradiative transition, which is mainly determined by acoustic phonons at low temperature. As the power of either $\boldsymbol{E}_1$ or $\boldsymbol{E}_2$ increases, such space (time delay) between two peaks [Fig. 2(c)] gets larger, which can be attributed to the energy-level splitting by the dressing effect [corresponding to the AT splitting in the spectrum in Fig. 2(a)]. The curves in Figs. 2(d) and 2(d) are the dressed PA FWM spectra together with their lifetimes corresponding to each fluorescence case [30]. Based on the analysis of the above florescence signals, one can easily determine the physical mechanism behind each output $\boldsymbol{E}_S$ as shown in Figs. 2(b) and 2(d). In other words, the dressing effect makes the intensity of the PA FWM decrease and the lifetime longer, whereas the dressing effect of the circularly polarized field is stronger than that for the linear case [20]. However, since the PA FWM signal is insensitive to the dressing field, there are no AT splittings in both the spectrum and time domain, as shown in Figs. 2(b) and 2(d), respectively.

Now, we focus on the intensity noise correlation and intensity-difference squeezing between the output beams $\boldsymbol{E}_S$ and $\boldsymbol{E}_{\mathrm{AS}}$ of the dressed PA FWM process as shown in Fig. 3. Figure 3(a) shows the noise correlations under various control conditions. First, the correlation levels at the resonance and off-resonance positions are different—the correlation is reduced at the suppression dip position [shown in Fig. 2(a), satisfying suppression condition $\Delta_1 - \Delta_2 = 0$; Fig. 2(a1), $\Delta_1 = 0$], while it is enlarged at the enhanced-peak position [shown in Fig. 2(a), satisfying the enhancement condition $\Delta_1 + \lambda_{\pm} = 0$; Fig. 2(a2), $\Delta_1 = 200$ GHz]. To investigate in detail the role of the dressed states on the correlation level, we plot a frequency dependence of the maximum correlation value on the discrete frequency detuning Δ_1 presented as square points in Fig. 3(b1). The two-mode correlation $G_{S,\mathrm{AS}}^{(2)}(\tau)$ [Eq. (11)] and squeezing (sq) [Eq. (12)] are determined by the nonlinear gains in Eq. (8), which can be modified by the dressing effect in Eqs. (9), (10), and (13) [31]. The curve includes three regions: the resonance, near resonance, and far off resonance, respectively. At the far off resonance, the nesting double-dressing configuration [d_{21D} and d_{20D} in Eqs. (9) and (10)] reduces to zero, and the nonlinear gain [Eq. (8)] gets the maximum value. At last, the maximum correlation is obtained. As Δ_1 is close to being near resonance, the correlation value becomes smaller and smaller due to the nonlinear gain (g) decrease, and the correlation reaches its minimum value at $\Delta_1 = 100$ GHz. Similarly, the correlation value is minimized at $\Delta_1 = -100$ GHz [the square points in Fig. 3(b1)]. However, in the region $|\Delta_1| \leq 100$ GHz, the dressing effect due to $\boldsymbol{E}_2$ cannot be neglected. Therefore, at resonance, the nesting double-dressing configuration (d_{20} and d_{21}) makes the correlation much smaller but not to its minimum value due to the action of dressing field $\boldsymbol{E}_2$, as shown in the square points in Fig. 3(b1). In addition, the modulated correlation time has the opposite behavior depicted with circular points in Fig. 3(b1). The single-dressing effect can result in the increased lifetime of the PA FWM and the decreased intensity of the PA FWM process [29]. The lifetime of the PA FWM process is inversely proportional to the decay rate of the PA FWM process, where the dressing results between the lifetime of the PA FWM process and the correlation time of $G_{S,\mathrm{AS}}^{(2)}(\tau)$ are coincident with each other because the lifetime of the PA FWM process [Fig. 2(d)] is modulated in the same way as shown in the circular curve in Fig. 3(b1). As we discuss above, the correlation time and

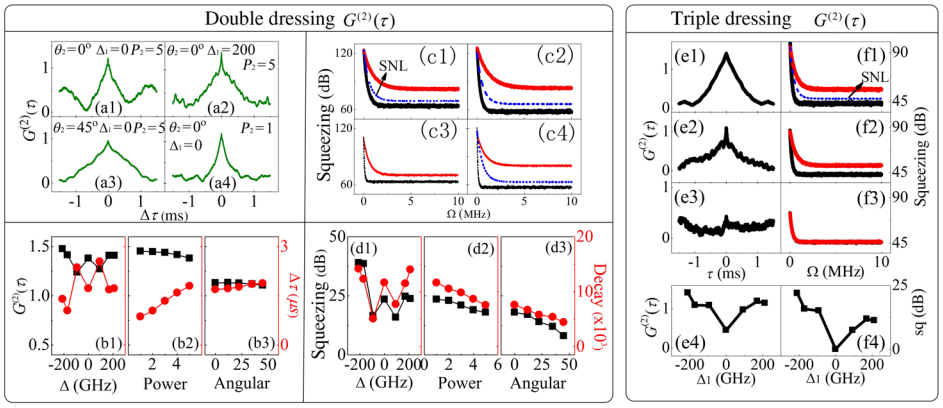

FIG. 3. Measured intensity noise correlation and squeezing. (a),(c) Measured intensity noise correlation and intensity-difference squeezing between output beams $\boldsymbol{E}_S$ and $\boldsymbol{E}_{\rm AS}$, where the PA FWM process is dressed by $\boldsymbol{E}_2$. All experimental conditions are identical except Δ_1 [(a1), $\Delta_1 = 0$] and [(a2), $\Delta_1 = 200$ GHz], polarization state of the dressing field $\boldsymbol{E}_2$ (a1) $\theta_2 = 0°$ and (a3) $\theta_2 = 45°$, and $\boldsymbol{E}_2$ power (a1) $P_2 = 5$ mW, and (a4) $P_2 = 1$ mW, respectively. (b) Frequency detuning, power and polarization dependences of the maximum correlation value $G^{(2)}(0)$ (squares), and correlation time $\Delta\tau$ (circles). (d) Dependences of the squeezing value at the analysis frequency 1.5 MHz (squares) and decay rate (circles) of the output beam $\boldsymbol{E}_S$, respectively, corresponding to the cases in (b). Note that the squares denote the case dressed by $\boldsymbol{E}_3$. (e),(f) Measured intensity noise correlation and intensity-difference squeezing between output beams $\boldsymbol{E}_S$ and $\boldsymbol{E}_{\rm AS}$ at (1) $\Delta_1 = 200$ GHz, (2) 60 GHz, and (3) 0, which are dressed by $\boldsymbol{E}_2$ and $\boldsymbol{E}_3$ simultaneously. (4) Frequency dependence of the maximum correlation and squeezing degree on the frequency detuning Δ_1.

decay rate are still valid, as shown by the circular points in Figs. 3(b2), 3(b3), and 3(d2), and 3(d3), and the degree of correlation [square points in Fig. 3(b)] is inversely proportional to the correlation time [circular points in Fig. 3(b)]. Now, we use the Cauchy-Schwarz inequality $G^{(2)}_{S,\rm AS}(\tau_1) \leq 1$ to check our experimental result [Fig. 3(a2)]. The measured correlation at off resonance is about 1.5, which clearly violates of the Cauchy-Schwarz inequality, proving that there is a nonclassical correlation between $\boldsymbol{E}_S$ and $\boldsymbol{E}_{\rm AS}$.

Next, we focus on the power and polarization dependences of the intensity noise correlation on $\boldsymbol{E}_2$. Figures 3(a1) and 3(a4) show the correlation curves at high power ($P_2 = 5$ mW) and low power ($P_2 = 1$ mW), respectively, when $\Delta_1 = 0$ and $\theta_2 = 0°$ (linear polarization). As the power of the dressing field increases, the correlation increases at first due to the dominant gain by the terms d_{20} and d_{21}, and then it becomes worse due to the dressing effect from the dressed term in Eq. (9), as shown by the square points in Fig. 3(b2). Figures 3(a1) and 3(a3) show the correlation curves at linear polarization ($\theta_2 = 0°$) and circular polarization ($\theta_2 = 45°$), respectively, when $\Delta_1 = 0$ and $P_2 = 5$ mW. As site I of the Pr^{3+} ion is much more sensitive to the circular polarization, one finds a similar behavior [see the square points in Fig. 3(b3)]. The competition between the linear component $C^2_{g2,\rm lin}(\cos^4\theta + \sin^4\theta)|G_2|^2$ and circular component $C^2_{g2,\rm cir}(2\cos^2\theta\sin^2\theta)|G_2|^2$ can well interpret such phenomena. Considering the relationship $\kappa \propto \chi^{(3)}_i \propto \rho^{(3)}$, the nonlinear gain can be modified by the polarizations of the dressing fields ($\boldsymbol{E}_2$ or $\boldsymbol{E}_3$). Specifically, the intensity ($|\rho^{(3)}|^2$) of the PA FWM is suppressed when the polarization of the dressing field changes from linear to circular due to the stronger dressing effect in the circular case. Therefore, $|\Psi_{s-as}|^2$ in Eq. (11) becomes smaller, and this leads to a lower correlation degree than that for the linearly polarized case [Figs. 3(a1) and 3(a3)]. Similarly, according to Eq. (12), the degree of squeezing decreases when the dressing field is circularly polarized compared with the linear case [Figs. 3(b1) and 3(b3)].

Figure 3(c) shows the intensity-difference squeezing (lowest curve in each panel) in contrast to the total noise (highest curve in each panel) or the shot-noise level [middle curve in Fig. 3(c2)]. Specifically, the highest curve in each panel is the total noise of the two output beams. The shot-noise level (SNL) [dashed curves in Figs. 3(c) and 3(f)] for the PA FWM process is defined as the intensity-difference noise on a pair of equal power beams produced from a coherent laser by a beam splitter with equal power as the sum of $\boldsymbol{E}_S$ and $\boldsymbol{E}_{\rm AS}$ [23]. As shown in Fig. 3(c2), the intensity-difference squeezing measured here is −4.5 dB, which is lower than the SNL. One finds that the double-dressing results of squeezing [Eq. (12)] have the same behavior as the correlation [Eq. (11)], which are determined by the dressed nonlinear gain in Eq. (8), as shown by the square points in each panel in Fig. 3(d). Therefore, the degree of intensity-difference squeezing of the output beams $\boldsymbol{E}_S$ and $\boldsymbol{E}_{\rm AS}$ depends crucially on the correlation functions [27,28].

When the dressing fields $\boldsymbol{E}_2$ and $\boldsymbol{E}_3$ are turned on simultaneously, a triple-dressed PA FWM process can be obtained [32]. Different from the case of the double-dressed PA FWM, the dressed results in Eq. (12) can be switched at $\Delta_1 = 0$. For example, the correlation measured here is

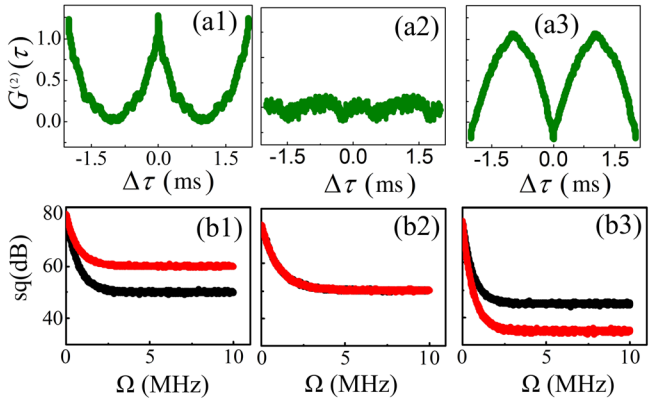

FIG. 4. (a) Intensity noise correlation curves between $\boldsymbol{E}_S$ and $\boldsymbol{E}_{\mathrm{AS}}$ versus delayed time τ with changing power of $\boldsymbol{E}_2$, with (a1) 6 mW, (a2) 8 mW, and (a3) 12 mW, respectively. (b1) $P_2 =$ 6 mW and $\omega = 1.5$ MHz. The lower curve and upper curve are the noise level of intensity-difference squeezing and intensity-sum squeezing versus analysis frequency Ω, respectively. (b2) $P_2 = 8$ mW. The intensity-sum squeezing and intensity-difference squeezing have the same noise level and are indistinguishable. (b3) $P_2 = 12$ mW and $\omega = 1.5$ MHz. The lower curve and upper curve are the noise level of the intensity-sum squeezing and intensity-difference squeezing, respectively.

about 1.4 [Fig. 3(e1)], which is reduced in comparison with that in Fig. 3(a1). However, there is also a nonclassical correlation between $\boldsymbol{E}_S$ and $\boldsymbol{E}_{\mathrm{AS}}$, since the Cauchy-Schwarz inequality is violated clearly. On the other hand, due to the different polarization responses of site I and site II, the frequency dependence of the maximum correlation value on Δ_1 presents an inverted Lorentzian line shape [see Fig. 3(e4)], while the double-dressed case is a normal Lorentzian line shape with a central peak [see Fig. 3(b1)]. Similar behaviors can be found for the intensity-difference squeezing [Eq. (13)] as shown in Fig. 3(f4) (triple dressed) and Fig. 3(d1) (double dressed). Thus, the intensity-difference squeezing [Figs. 3(d) and 3(f4)] is proportional to the corresponding noise correlation [Figs. 3(b) and 3(e4)] of the PA FWM process.

In addition, we not only verify that the intensity-difference squeezing and intensity noise correlation can be easily manipulated by several parameters in Fig. 3, but we also show that the correlation and squeezing can be controlled by the relative nonlinear phase shift caused by the dressing beam. As shown in Fig. 4(a1), with $P_2 = 6$ mW, the amplitude of the correlation peak at delay time $\tau = 0$ is 1.3. The Cauchy-Schwarz inequality is violated in Fig. 4(a1) and nonclassical correlation between $\boldsymbol{E}_S$ and $\boldsymbol{E}_{\mathrm{AS}}$ is demonstrated. As $P_2 = 8$ mW, the amplitude is about 0, as shown in Fig. 4(a2), and there do not exist correlation and squeezing. In particular, the intensity fluctuation is switched from correlated to anticorrelated if $P_2 = 12$ mW, as shown in Fig. 4(a3). These results can be explained by the nonlinear refractive index of the Kerr medium. Since the dressing state created by $\boldsymbol{E}_2$ can modulate the nonlinear refractive index of the Kerr medium that results from the cross-phase modulation (XPM), the relative nonlinear phase $\Delta\varphi = \varphi_S - \varphi_{\mathrm{AS}} = 2(k_S n_2^S - k_{\mathrm{AS}} n_2^{\mathrm{AS}})|E_2|^2 e^{-r^2} z/n_1$ between the Stokes and anti-Stokes signals is significantly modulated. Here, φ_S (φ_{AS}) is the nonlinear phase induced on the Stokes (anti-Stokes) signal. The Kerr effect is associated with nonlinear refractive index n_2 (corresponding to the third-order nonlinear response) and intensity of light I ($n_2 I$, $n_2 = \mathrm{Re}\chi^{(3)}/\varepsilon_0 c n_1$). To be specific, by setting $P_2 = 6$, 8, and 12 mW, the relative nonlinear phase $\Delta\varphi$ changes to $\Delta\varphi = 0$, $\pi/2$, and π, respectively. Correspondingly, the correlation [Eq. (12)] switches from positive to zero and then to negative. Moreover, by changing $\Delta\varphi$, Figs. 4(b1)–4(b3) show that the intensity-difference signal [Eq. (13)] can be switched to either higher or lower than the total noise signal, which corresponds to squeezing or antisqueezing, respectively. Therefore, the intensity fluctuation correlation and the intensity-difference squeezing of the output beams $\boldsymbol{E}_S$ and $\boldsymbol{E}_{\mathrm{AS}}$ depend crucially on the relative nonlinear phase induced by XPM.

C. Triplet beams by the PA SWM process

Furthermore, we investigate the three-mode correlation and squeezing of the PA SWM with an injecting coherent FWM. Different from the generated twin beams by the SP FWM process, laser fields $\boldsymbol{E}_2$ and $\boldsymbol{E}_3$ both at large detunings are set to be certain angles with $\boldsymbol{E}_1$ satisfying the phase-matching condition. Thus, mutually correlated triplet beams can be produced by a SP SWM process with the phase-matching condition $\mathbf{k}_{S1} + \mathbf{k}_{S2} + \mathbf{k}_{S3} = \mathbf{k}_1 + \mathbf{k}_2 + \mathbf{k}_3$. Since such SP SWM process [14] can be mimicked by cascading two involved closed-loop SP FWM processes ($\mathbf{k}_{S1} + \mathbf{k}_{S2} = \mathbf{k}_1 + \mathbf{k}_2$ and $\mathbf{k}_{S1} + \mathbf{k}_{S3} = \mathbf{k}_1 + \mathbf{k}_3$) [Fig. 5(a)], one can write the Hamiltonian as $H_I = i\hbar\kappa_1 \hat{a}_{S1}^{\dagger}\hat{a}_{S2}^{\dagger} + i\hbar\kappa_2 \hat{a}_{S1}^{\dagger}\hat{a}_{S3}^{\dagger} + \mathrm{H.c.}$, where $\hat{a}_{S1}^{+}, \hat{a}_{S2}^{+}, \hat{a}_{S3}^{+}$ are the boson creation operators of the three generated fields, and $\kappa_1 = -i\varpi_{S1}\chi_1^{(3)} E_1 E_2/2$ and $\kappa_2 = -i\varpi_{S1}\chi_2^{(3)} E_1 E_3/2$ are the third-order nonlinear susceptibility of

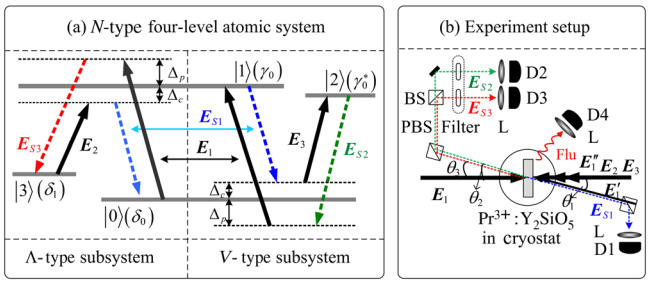

FIG. 5. (a) N-type four-level atomlike system in $Pr^{3+}:Y_2SiO_5$ for triple-photon generation by a SP SWM process composed of Λ-type and V-type three-level subsystems. (b) New experimental scheme for the SP SWM process with the phase-matching condition $\mathbf{k}_{S1} + \mathbf{k}_{S2} + \mathbf{k}_{S3} = \mathbf{k}_1 + \mathbf{k}_2 + \mathbf{k}_3$.

cascading two ($\chi_1^{(3)}$ and $\chi_2^{(3)}$) involved SP FWM processes. Therefore, one can easily get the dynamic equations as

$$\begin{aligned} d\hat{a}_{S2}/dt &= \kappa_1 \hat{a}_{S1}^{\dagger}, \\ d\hat{a}_{S1}/dt &= \kappa_1 \hat{a}_{S2}^{\dagger} + \kappa_2 \hat{a}_{S3}^{\dagger}, \\ d\hat{a}_{S3}/dt &= \kappa_2 \hat{a}_{S1}^{\dagger}. \end{aligned} \tag{14}$$

Similar to the PA FWM process, one can calculate the output results from these equations. Here, we are concerned about the properties of the output signals from this PA SWM process with an injecting coherent FWM ($\mathbf{k}_F = \mathbf{k}_1 + \mathbf{k}_1'' - \mathbf{k}_1'$) [15], and then we extend the $G^{(2)}(\tau)$ function for the two-mode case to the three-mode correlation function $G^{(3)}(\tau)$ as

$$G^{(3)} = \frac{\langle [\delta \hat{I}_{S1}(t_{S1})][\delta \hat{I}_{S2}(t_{S2})][\delta \hat{I}_{S3}(t_{S3})] \rangle}{\sqrt{\langle [\delta \hat{I}_{S1}(t_{S1})]^2 \rangle \langle [\delta \hat{I}_{S2}(t_{S2})]^2 \rangle \langle [\delta \hat{I}_{S3}(t_{S3})]^2 \rangle}} = \frac{(H_{S1S2S3} - H_{S3}C_{S1S2} - H_{S2}C_{S1S3} - H_{S1}C_{S3S2} + 2H_{S1}H_{S2}H_{S3})}{\sqrt{|C_{S1}|^2(|C_{S2}|^2 + |C'_{S2}|^2)|C_{S3}|^2}}, \tag{15}$$

where H_{S1S2S3} is the cross-correlation function of intensity between $\boldsymbol{E}_{S1}$, $\boldsymbol{E}_{S2}$, and $\boldsymbol{E}_{S3}$, and H_{Si} is the one-order correlation function of the intensity. C_{SiSj} is the cross-correlation function between the intensity fluctuations of $\boldsymbol{E}_{Si}$ and $\boldsymbol{E}_{Sj}$ ($i, j = 1, 2, 3, i \neq j$). $\mathbf{C}_{Si}$ is the self-correlation function. The conditional intensity-difference squeezing for the three-mode case can be given by [24,31]

$$\mathrm{sq} = \log_{10} \frac{\langle \delta^2(\hat{N}_{S1} - \hat{N}_{S2} - \hat{N}_{S3}) \rangle}{\langle \delta^2(\hat{N}_{S1} + \hat{N}_{S2} + \hat{N}_{S3}) \rangle} \approx 2\log_{10} \frac{g_1^2 - g_2^2 - g_3^2}{g_1^2 + g_2^2 + g_3^2}, \tag{16}$$

where $g_1 = [\kappa_2^2 + \kappa_1^2 \cosh(\Omega L)]/(\kappa_2^2 + \kappa_1^2)$, $g_2 = \kappa_1 \sinh(\Omega L)/\sqrt{\kappa_2^2 + \kappa_1^2}$, and $g_3 = \kappa_1\kappa_2(\cosh(\Omega L) - 1)/\kappa_2^2 + \kappa$.

When beams $\boldsymbol{E}_1$, $\boldsymbol{E}_2$, and $\boldsymbol{E}_3$ are turned on simultaneously, as shown in Fig. 5(a), a PA SWM process with the phase-matching condition $\mathbf{k}_{S1} + \mathbf{k}_{S2} + \mathbf{k}_{S3} = \mathbf{k}_1 + \mathbf{k}_2 + \mathbf{k}_3$ can be obtained in the N-type four-level system. Figure 5(b) shows the experimental arrangement for meeting the PA SWM phase-matching condition. To satisfy the requirement for such PA SWM process, two PA FWM processes share the pumping beam $\boldsymbol{E}_1$ and output beam $\boldsymbol{E}_{S1}$ in both the frequency domain and spatial domain by using a specially designed experimental configuration (fields $\boldsymbol{E}_2$ and $\boldsymbol{E}_3$ both counterpropagating with $\boldsymbol{E}_1$ at a certain angle to meet the phase-matching condition). The major difference between the current PA SWM experimental scheme [Fig. 5(a)] and that in Fig. 1(a) is the frequency detuning set for $\boldsymbol{E}_1$, $\boldsymbol{E}_2$, and $\boldsymbol{E}_3$. In addition, due to the angle between $\mathbf{k}_2$, $\mathbf{k}_3$, and $\mathbf{k}_1$, the generated SWM signal cannot be obtained in the same direction of the FWM when the detector is placed as shown in Fig. 1(a). Therefore, $\boldsymbol{E}_2$ and $\boldsymbol{E}_3$ are only dressing fields for the SP FWM in Fig. 1(a) while $\boldsymbol{E}_1$, $\boldsymbol{E}_2$, and $\boldsymbol{E}_3$ are all generating fields for the SP SWM.

Figure 6 depicts the triple-beam correlation and intensity-difference squeezing results. Two sets of frequency detunings of $\boldsymbol{E}_1$ are set at off resonance [$\Delta_1 = 200$ GHz, Fig. 6(a)] and on resonance [$\Delta_1 = 0$, Fig. 6(b)], respectively. Three-mode correlation [Eq. (15)] and squeezing [Eq. (16)] are determined by the dressed nonlinear gains [31]. By comparing the results of triple-beam correlation and intensity-difference squeezing, one finds that the maximum correlation value at off resonance is bigger than the on-resonance case, which is similar to that shown for the twin beams. However, the correlation level is weaker than that for the case of triple-dressed twin beams since the correlation condition is more stringent as shown in Eq. (15). Similar behavior occurs with the intensity-difference squeezing. In contrast to the twin beams, the SNL for the PA SWM process becomes the intensity-sum noise on three coherent laser beams with equal power as the sum of $\boldsymbol{E}_{S1}$, $\boldsymbol{E}_{S2}$, and $\boldsymbol{E}_{S3}$. In Eq. (16), $\langle \delta^2(\hat{N}_{S1} + \hat{N}_{S2} + \hat{N}_{S3}) \rangle$

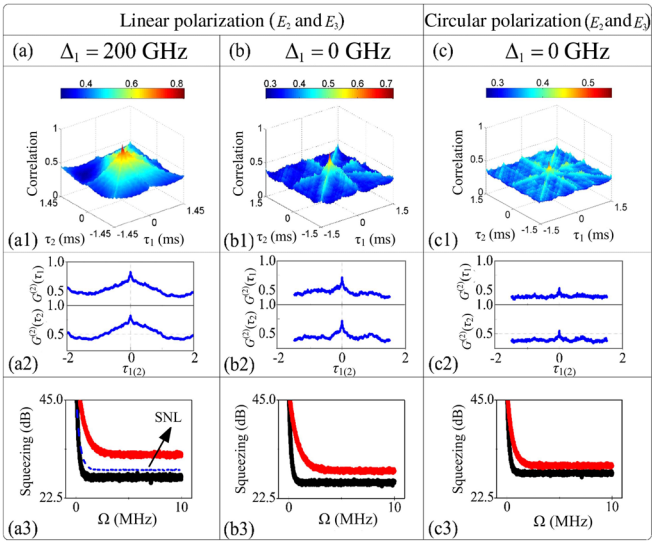

FIG. 6. Three-mode noise correlation and intensity-difference squeezing of $\boldsymbol{E}_{S1}$, $\boldsymbol{E}_{S2}$, and $\boldsymbol{E}_{S3}$. Experimental conditions are set as follows: (a),(b) $\boldsymbol{E}_1$, $\boldsymbol{E}_2$, and $\boldsymbol{E}_3$ are linearly polarized, (c) $\boldsymbol{E}_1$ is linearly polarized, while $\boldsymbol{E}_2$ and $\boldsymbol{E}_3$ are circularly polarized.

is the total noise of the three coherent laser beams. Based on the cascade processes [24], $\langle\delta^2(\hat{N}_{S1}-\hat{N}_{S2}-\hat{N}_{S3})\rangle$ is the intensity noise difference of three output beams. Because of the more stringent condition of the three-mode direct correlation, the squeezing value is smaller than in the dressed twin-beam case. We get a −3.5 dB squeezing in Fig. 6(a3), but the same role played by the dressed state is still true for the squeezing results; i.e., it reduces the squeezing.

Next, we focus on the case when both $\boldsymbol{E}_2$ and $\boldsymbol{E}_3$ are either linearly polarized [Fig. 6(b)] or circularly polarized [Fig. 6(c)] while $\boldsymbol{E}_1$ remains linearly polarized. Apparently, the correlation and squeezing with linear polarization are better than the case with circular polarization, which is similar to the twin-beam case with single dressing field $\boldsymbol{E}_2$ only (Fig. 3).

IV. CONLUSIONS

We investigate the generated twin beams by the PA FWM process and triplet beams by the PA SWM process associated with the MFL signals in a $PR^{3+}:Y_2SiO_5$ crystal. First, the degrees of intensity noise correlation and intensity-difference squeezing between the output beams $\boldsymbol{E}_S$ and $\boldsymbol{E}_{\mathrm{AS}}$ of the PA FWM process are determined by the nonlinear gain, which can be controlled by the dressing variables. The correlation at the resonant position can attain a higher value due to the double-dressing effect; however, such correlation is reduced in the case of the triple-dressing effect. Second, the correlation of the PA FWM can change to anticorrelation by the nonlinear phase shift, which is induced by the external dressing beam, and the noise level of the intensity-difference squeezing is switched synchronously. Finally, we investigate the intensity noise correlation and intensity-difference squeezing of the triplet beams generated by the PA SWM process, which is well interpreted by two cascaded nonlinear processes. The correlation level is weaker than the case of twin beams since the three-mode correlation condition is more stringent. Meanwhile, the squeezing value is also smaller than the twin-beam case. Similarly, the polarized dark state still plays the same role in the results. Such results can find potential applications in engineering three-channel entangled imaging on chip.

ACKNOWLEDGMENTS

This work is supported by the National Natural Science Foundation of China (Grant Nos. 11474228, 61605154), Key Scientific and Technological Innovation Team of Shaanxi Province (Grant No. 2014KCT-10), China Postdoctoral Science Foundation (Grant Nos. 2016M590935, 2016M600777, 2016M600776).

[1] V. Berger, Nonlinear Photonic Crystals, Phys. Rev. Lett. **81**, 4136 (1998).
[2] N. G. R. Broderick, G. W. Ross, H. L. Offerhaus, D. J. Richardson, and D. C. Hanna, Hexagonally Poled Lithium Niobate: A Two-Dimensional Nonlinear Photonic Crystal, Phys. Rev. Lett. **84**, 4345 (2000).
[3] H. Jin, P. Xu, X. W. Luo, H. Y. Leng, Y. X. Gong, W. J. Yu, M. L. Zhong, G. Zhao, and S. N. Zhu, Compact Engineering of Path-Entangled Sources from a Monolithic Quadratic Nonlinear Photonic Crystal, Phys. Rev. Lett. **111**, 023603 (2013).
[4] Y. Zhao, C. Wu, B. Ham, M. Kim, and E. Awad, Microwave Induced Transparency in Ruby, Phys. Rev. Lett. **79**, 641 (1997).
[5] M. Phillips, H. Wang, I. Rumyantesev, N. Kwong, R. Takayama, and R. Binder, Electromagnetically Induced Transparency in Semiconductors via Biexciton Coherence, Phys. Rev. Lett. **91**, 183602 (2003).
[6] A. Turukhin, V. Sudarshanam, M. Shahriar, J. Musser, B. Ham, and P. Hemmer, Observation of Ultraslow and Stored Light Pulses in a Solid, Phys. Rev. Lett. **88**, 023602 (2001).
[7] J. Longdell, E. Fraval, M. Sellars, and N. Manson, Stopped Light with Storage Times Greater than One Second Using Electromagnetically Induced Transparency in a Solid, Phys. Rev. Lett. **95**, 063601 (2005).
[8] G. Heinze, C. Hubrich, and T. Halfmann, Stopped Light and Image Storage by Electromagnetically Induced Transparency up to the Regime of One Minute, Phys. Rev. Lett. **111**, 033601 (2013).
[9] J. L. O'Brien, Optical quantum computing, Science **318**, 1567 (2007).
[10] J. L. O'Brien, G. J. Pryde, A. G. White, T. C. Ralph, and D. Branning, Demonstration of an all-optical quantum controlled-NOT gate, Nature (London) **426**, 264 (2003).
[11] H. H. Wang, A. J. Li, D. M. Du, Y. F. Fan, L. Wang, Z. H. Kang, Y. Jiang, J. H. Wu, and J. Y. Gao, All-optical routing by light storage in a crystal, Appl. Phys. Lett. **93**, 221112 (2008).
[12] B. S. Ham, M. S. Shahriar, and P. R. Hemmer, Enhancement of four-wave mixing and line narrowing by use of quantum coherence in an optically dense double-Λ solid, Opt. Lett. **24**, 86 (1999).
[13] R. W. Equall, R. L. Cone, and R. M. Macfarlane, Homogeneous broadening and hyperfine structure of optical transitions in $Pr^{3+}:Y_2SiO_5$, Phys. Rev. B **52**, 3963 (1995).
[14] D. Zhang, H. Y. Lan, C. B. Li, H. B. Zheng, C. J. Lei, R. M. Wang, I. Metlo, and Y. P. Zhang, Observation of Autler-Townes splitting of second-order fluorescence in Pr^{3+}:YSO, J. Phys. Chem. C **118**, 14521 (2014).
[15] H. B. Zheng, X. Zhang, Z. Y. Zhang, Y. L. Tian, H. X. Chen, C. B. Li, and Y. P. Zhang, Parametric amplification and cascaded-nonlinearity processes in common atomic system, Sci. Rep. **3**, 1885 (2013).
[16] Z. Q. Nie, H. B. Zheng, P. Z. Li, Y. M. Yang, Y. P. Zhang, and M. Xiao, Interacting multi-wave mixing in a five-level atomic system, Phys. Rev. A **77**, 063829 (2008).

[17] J. Sun, Z. C. Zuo, X. Mi, Z. H. Yu, Q. Jiang, Y. B. Wang, L. A. Wu, and P. M. Fu, Phys. Rev. A **70**, 053820 (2004).
[18] J. M. Wen, S. W. Du, Y. P. Zhang, M. Xiao, and M. H. Rubin, Nonclassical light generation via a four-level inverted-*Y* system, Phys. Rev. A **77**, 033816 (2008).
[19] H. X. Chen, M. Z. Qin, Y. Q. Zhang, X. Zhang, F. Wen, J. M. Wen, and Y. P. Zhang, Laser Phys. Lett. **11**, 045201 (2014).
[20] C. B. Li, Y. P. Zhang, Z. Q. Nie, Y. G. Du, R. M. Wang, J. P. Song, and M. Xiao, Controlling enhancement and suppression of four-wave mixing via polarized light, Phys. Rev. A **81**, 033801 (2010).
[21] H. Wu and M. Xiao, Bright correlated twin beams from an atomic ensemble in the optical cavity, Phys. Rev. A **80**, 063415 (2009).
[22] S. W. Du, J. M. Wen, M. H. Rubin, and G. Y. Yin, Four-Wave Mixing and Biphoton Generation in a Two-Level System, Phys. Rev. Lett. **98**, 053601 (2007).
[23] V. Boyer, A. M. Marino, R. C. Pooser, and P. D. Lett, Entangled images from four-wave mixing, Science **321**, 544 (2008).
[24] Z. Z. Qin, L. M. Cao, H. L. Wang, A. M. Marino, W. P. Zhang, and J. T. Jing, Experimental Generation of Multiple Quantum Correlated Beams from Hot Rubidium Vapor, Phys. Rev. Lett. **113**, 023602 (2014).
[25] Robert W. Boyd, Michelle S. Malcuit, Daniel J. Gauthier, and K. Rzazewski, Competition between amplified spontaneous emission and the four-wave-mixing process, Phys. Rev. A **35**, 1648 (1987).
[26] J. Qi, F. C. Spano, T. Kirova, A. Lazoudis, J. Magnes, L. Li, L. M. Narducci, R. W. Field, and A. M. Lyyra, Measurement of Transition Dipole Moments in Lithium Dimers Using Electromagnetically Induced Transparency, Phys. Rev. Lett. **88**, 173003 (2002).
[27] F. Boitier, A. Godard, E. Rosencher, and C. Fabre, Measuring photon bunching at ultrashort timescale by two-photon absorption in semiconductors, Nat. Phys. **5**, 267 (2009).
[28] F. Boitier, A. Godard, N. Dubreuil, P. Delaye, C. Fabre, and E. Rosencher, Photon extrabunching in ultrabright twin beams measured by two-photon counting in a semiconductor, Nat. Commun. **2**, 425 (2011).
[29] H. B. Zheng, C. B. Li, H. Y. Lan, C. J. Lei, D. Zhang, Y. P. Zhang, and M. Xiao, Seeded spontaneous parametric four-wave mixing and fluorescence of Pr^{3+}:YSO, Laser Phys. Lett. **11**, 116102 (2014).
[30] I. Ali, C. B. Li, A. Hasan, G. Abdisa, Z. C. Liu, F. Ma, and Y. P. Zhang, Lifetime Autler-Townes splitting of dressed multi-order fluorescence in Pr^{3+}:YSO, Front. Phys. **4**, 32 (2016).
[31] Y. F. Zhang, D. Zhang, H. Y. Zhang, H. J. Tang, L. Cheng, R. Z. Liu, and Y. P. Zhang, Dressing control of three-mode entanglement in two cascaded four-wave mixing, Laser Phys. Lett. **13**, 115201 (2016).
[32] P. Y. Li, H. B. Zheng, Y. Q. Zhang, J. Sun, C. B. Li, G. P. Gao, Z. Y. Zhang, Y. Y. Li, and Y. P. Zhang, Controlling the transition of bright and dark states via scanning dressing field, Opt. Mater. **35**, 1062 (2013).